Integrative prototype *B*-scan photoacoustic tomography system based on a novel hybridized scanning head

Diwu Yang,[a] Da Xing,[b] Yi Tan, Huaimin Gu, and Sihua Yang
MOE Key Labratory of Laser Life Science & Institute of Laser Life Science, South China Normal University, Guangzhou 510631, China

(Received 10 January 2006; accepted 11 March 2006; published online 24 April 2006)

A prototype *B*-scan photoacoustic tomography system is developed. It integrates pumping fiber, ultrasound coupling medium, and a transducer array into a novel hybridized scanning head. By moving the scanning head a photoacoustic tomography can be obtained in the reflection mode. Concentration-adjustable glycerite is used as the ultrasonic coupling medium to match the ultrasonic velocities in tissues, reducing the acoustic reflection, eliminating the acoustic refraction, and rectifying the acoustic path difference. This system is used to image graphite phantom in tissue and human blood vessels. Our experimental results show that this integrative system has the potential for fast photoacoustic imaging. © *2006 American Institute of Physics*. [DOI: 10.1063/1.2198488]

Photoacoustic (PA) effect is based on irradiating absorbers with time-resolved light.[1] Absorption of the light results in a rapid thermoelastic expansion, which leads to an initial stress distribution. The ultrasonic waves propagate to the surface and can be detected by highly sensitive piezoelectric devices outside the tissue. The optical absorption heterogeneity inside tissues can be reconstructed from the detected time-resolved PA signals. This imaging method combines the advantages of optic imaging and ultrasonic imaging, and can acquire images with high resolution and high contrast.[2,3] The light absorption of tissue not only reflects its characteristic structure but also its metabolic and characteristic pathological changes, because different tissues in different physiology conditions have different light absorption coefficients.[4,5] For example, the absorption contrast between breast tumor and normal breast tissue can be as high as 500% at the near infrared range.[6]

In the past decade, a number of papers describing PA imaging techniques have been published.[7–13] In these experiments, the reconstructed image can map the distribution of the radiation absorption within the samples, but there are still problems to be resolved. Firstly, the long acquisition time caused by scanning and averaging or the mechanical complication of experimental setup hinders the practical application of PA imaging. Secondly, the fact that the acoustic reflectance and refraction in the interface of two different media are caused in virtue of mismatching of acoustic velocities and acoustic impedance during the propagation of acoustic waves has not been taken into consideration. Thirdly, in the clinic application of photoacoustic imaging, most human body parts are not accessible from two sides; therefore laser illumination and acoustic sensing need to be on the same side.

We have constructed an integrative prototype *B*-scan photoacoustic tomography system with a novel hybridized scanning head, which integrates pumping fiber, ultrasound coupling medium, and a multielement linear transducer array into a portable scanning head. To our best knowledge, the concentration-adjustable glycerite is used for the first time as an ultrasound coupling medium to match the ultrasonic velocities in tissues. The system collected PA signals in the reflection mode with the multielement phase-controlled technique,[14,15] and PA images were reconstructed with the limited-field filtered back projection algorithm.[14] PA images of phantom lard at different depths and blood vessels *in vivo* on the forearm of a volunteer were obtained with the system.

Acoustic refraction and reflection are generated when PA wave propagates through the interface of two different media. . According to the relative theory of acoustics, the following equations can be obtained:

$$n_{12} = \frac{\sin\theta}{\sin\varphi} = \frac{c_2}{c_1}, \tag{1}$$

$$R_p = \frac{\rho_1 c_1 \cos\theta - \rho_2 c_2 \cos\varphi}{\rho_1 c_1 \cos\theta + \rho_2 c_2 \cos\varphi}, \tag{2}$$

where c_1 and c_2 are the acoustic velocities in the two media, θ and φ are the incident angle and the reflected angle, and ρ_1 and ρ_2 are the densities of the two media, respectively. From Eq. (1), it can be found that the refraction is determined by the acoustic velocities in the two media. If the velocities in the two media are the same, the refraction in the interface of the two media can be avoided. From Eq. (2), when the acoustic velocities in the two media are matched, the reflectance coefficient R_p also decreases, so the reflectance in the interface can be reduced.

The integrative prototype *B*-scan photoacoustic tomography system includes a fiber [core diameter=600 μm, numerical aperture NA=0.22], a transducer array (PL-21; SIUI, China) with 320 vertical transducers, and an ultrasonic coupling medium (glycerin and water). The dimensions of the hybridized scanning head are 3.5, 8, and 10 cm, as shown in Fig. 1(a), and the height of the hybridized scanning head along the z axis is 4 cm. The schematic of the experimental setup is shown in Fig. 1(b). A Nd: YAG (yttrium aluminum garnet) laser (Brilliant B, Bigsky) with a wavelength of 1064 nm, output of 8 ns pulse width at 40 mJ/pulse, and repetition rate of 20 Hz was used to irradiate the sample. The resonance frequency of the transducer array is 7.5 MHz and the scanning width of the array is 49 mm. A built-in cylinder acoustic lens, made of silicon rubber with a focal length of 3.5 cm, was used to select the two-dimensional image plane and suppress out-of-plane signals. The fiber and the trans-

[a]Electronic mail: yangdw@scnu.edu.cn
[b]Author to whom correspondence should be addressed; FAX: +86-20-85216052; electronic mail: xingda@scnu.edu.cn

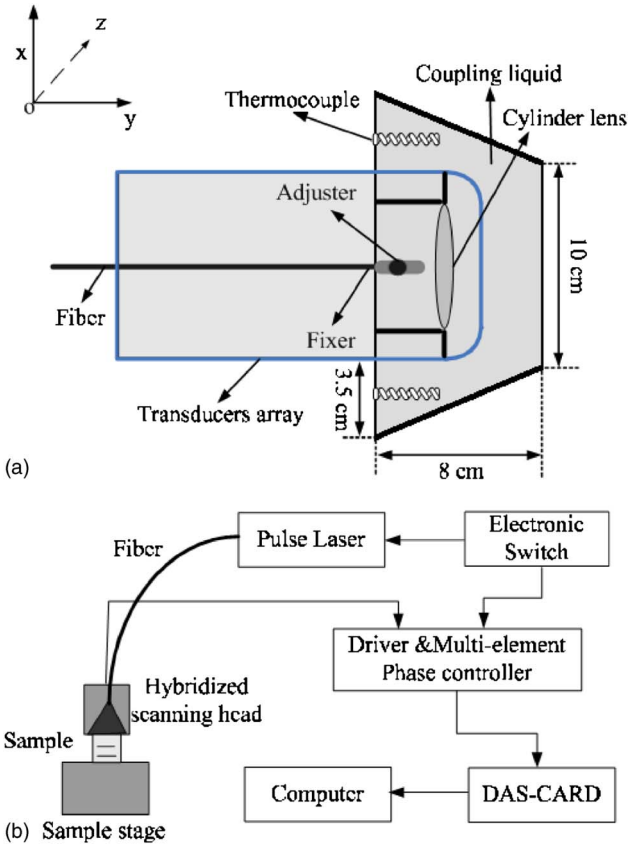

FIG. 1. (Color online) (a) Plan form of the hybridized scanning head. (b) Experimental setup of the integrative prototype *B*-scan photoacoustic tomography system.

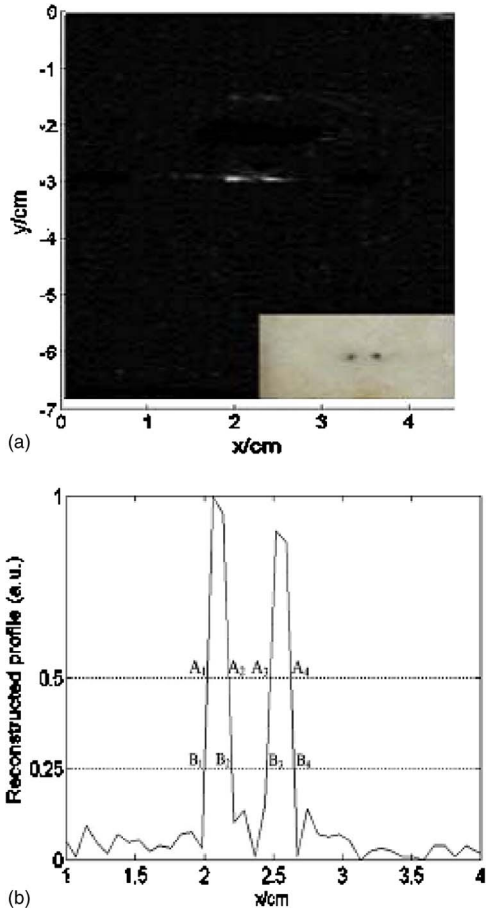

FIG. 2. (Color online) (a) Reconstructed image of the phantom. [Inset: cross section between the two graphite rods (diameter=0.7 mm; length=2 mm) inserted in the pork fatty tissue. The center distance between the two graphite rods was 3 mm.] (b) The normalization line profile of the reconstructed image in (a) at $y=3.1$ cm. The half-amplitude line and quarter-amplitude line cut across the profile at points A_{1-4} and B_{1-4}, respectively.

ducer array were fixed in a box and the angle between them was adjustable. The laser symmetrically irradiated the target tissues through a cylinder optical lens that focused the laser beam along the z axis to effectively reduce potential damage to tissues. The ultrasound velocity in the ultrasonic coupling medium was adjusted to be the same as that in the fatty tissue (1547 m/s). The glycerin concentration used in our experiments was 11.2%. There were two thermocouples placed at the side of the transducer array to ensure a steady temperature during the experiment.

The control circuit offered a pulse signal of 20 Hz. The signal was used to select one group of multielement linear transducers in order to receive the PA signals and synchronally control the *Q*-switched Nd: YAG laser. The transducer array detected the PA signals by using a multielement phase-controlled technique, then the detected PA signals were collected by a data acquisition system (DAS) card (Compuscope 12100; Gage Applied Co., Montreal, Quebec, Canada) and the data were stored in a personal computer. Finally, the PA image was reconstructed with the limited-field filtered back projection algorithm.

In order to estimate the resolution of the integrative prototype *B*-scan tomography system, in the first experiment two graphite rods (diameter=0.7 mm; length=2 mm; center distance between the two rods=3 mm) inserted in the pork fatty tissue were used. The feasibility of PA imaging at different depths of tissues was evaluated in our second experiment, using a long graphite rod (length=5.2 cm; diameter =0.7 mm) embedded in the lard sample with a horizontal angle of 22.6°. The depth of the graphite was 0.5–20 mm beneath the surface of the lard. In the third experiment, the PA images of branching cutaneous veins were obtained on the forearm of a volunteer. An arm support was used to keep the arm in a stable position during the measurement. The measurement consisted of eight linear scans with step of 3 mm along the arm direction, and the scanned region covered 2.1×1.6 cm^2.

Figure 2(a) shows the reconstructed image of fatty tissue with inserted graphite rods. Figure 2(b) is the normalization line profile of the reconstructed image at $y=3.1$ cm. The half-amplitude line and quarter-amplitude line cut across the profile at points A_{1-4} and B_{1-4} in Fig. 2(b). The spatial resolution of the imaging system is estimated according to the resolution criterion defined in the literature.[12] The value of system lateral resolution along the x axis is 0.28 mm.

Figure 3(a) is the photograph of the sample with the inserted long graphite rod. Figures 3(b) and 3(c) show the PA images of phantom at different positions with two scanning modes. For the image in Fig. 3(b), the hybridized scanning head was placed parallel to the x axis and it scanned along the y axis with a step of 1.2 cm. The PA images were obtained at five positions marketed as *A*, *B*, *C*, *D*, and *E* in Fig. 3(a). It can be found that the intensities of images decrease with the increment of the lard thickness due to the attenuation of laser energy and ultrasonic wave intensity. The fifth image in Fig. 3(b) is the reconstructed image of graphite with the depth of 20 mm, so the maximal depth of PA imag-

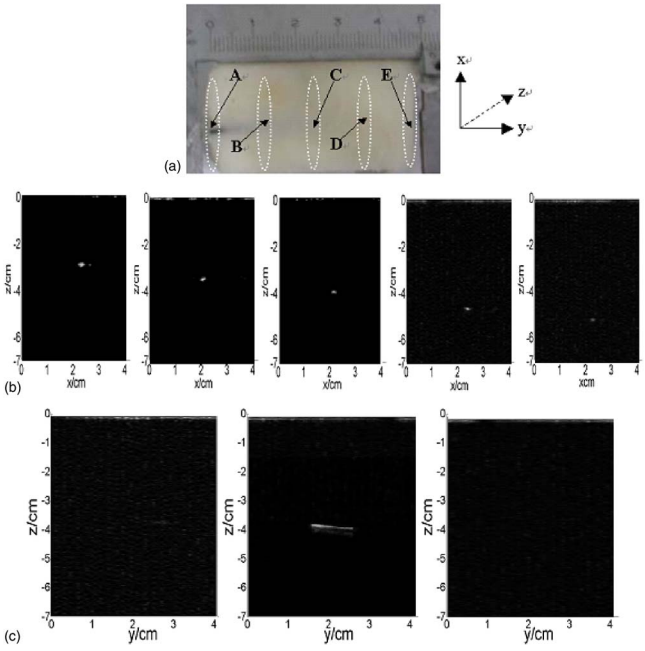

FIG. 3. (Color online) (a) Cross section of a tissue sample with the inserted long graphite rod. (b) The photoacoustic images of different tissue depths were obtained in five positions corresponding to areas *A*, *B*, *C*, *D*, and *E*. The hybridized scanning head was placed parallel to the *x* axis and it scanned along the *y* axis with a step of 1.2 cm. (c) The photoacoustic images were obtained in three sites. The hybridized scanning head was placed parallel to the *y* axis ($y=2.0-3.1$ cm) and it scanned along the *x* axis with the step of 0.8 cm.

ing can reach to at least 20 mm in lard. In Fig. 3(c), the PA images were obtained at three sites. The hybridized scanning head was placed parallel to the *y* axis and it scanned along the *x* axis with a step of 0.8 cm. The first and third images do not show the graphite rod; the second one is the reconstructed image of a fragment of the long graphite rod at the position of $y=2.0-3.1$ cm.

Figure 4 shows the photoacoustic image of two joining blood vessels on the forearm of a human volunteer. Figure 4(a) is the photograph of the scanned area, and 4(b) shows the reconstructed PA image of the blood vessels, which consists of eight slices. The image sequence was acquired by moving the hybridized scanning head 2.1 cm with a step of 3 mm along the forearm at a position 8.7 cm away from the wrist. It can be seen that the cross section of the blood vessels can be imaged with high contrast and spatial resolution, even the joined location of the vessels. Besides the blood vessels, the skin has also been imaged, due to the difference in optical absorptions between the skin and the coupling medium.

In conclusion, we have designed and assembled the integrative prototype *B*-scan photoacoustic tomography system, which effectively integrates the laser irradiation, photoacoustic coupling, and photoacoustic detection into a portable scanning head, and can quickly obtain the PA tomography sequence by conveniently moving the hybridized scanning head. This system combines the advantages of conventional ultrasound imaging and photoacoustic imaging. It has the potential to provide an effective approach for high-contrast vascular imaging.

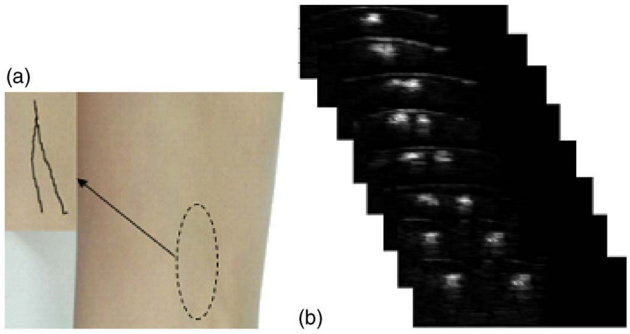

FIG. 4. (Color online) The photoacoustic image of two joining blood vessels on the forearm of a human volunteer. (a) is a photograph of the scanned area and (b) shows the reconstructed PA image of the blood vessels, which consists of eight slices.

This research is supported by the National Natural Science Foundation of China (60378043 and 30470494), and the Natural Science Foundation of Guangdong Province (015012, 04010394, and 2004B10401011).

[1]T. Bowen, Proc.-IEEE Ultrason. Symp. **2**, 817 (1981).
[2]G. Ku and L.-H. V. Wang, Med. Phys. **28**, 4 (2001).
[3]C. G. A. Hoelen, F. F. M. de Mul, R. Pongers, and A. Dekker, Opt. Lett. **23**, 648 (1998).
[4]A. A. Oraevaky, A. A. Karabutov, S. V. Solomatin, and E. V. Savateeva1, Proc. SPIE **4256**, 6 (2001).
[5]R. I. Siphanto, K. K. Thumma, R. G. M. Kolkman, T. G. van Leeuwen, F. F. M. de Mul, J. W. van Neck, L. N. A. van Adrichem, and W. Steenbergen, Opt. Express **13**, 89 (2005).
[6]K. Suzuki, Y. Yamashita, K. Ohta, M. Kaneko, M. Yoshida, and B. Chance, J. Biomed. Opt. **1**, 330 (1996).
[7]R. A. Kruger, P. Y. Liu, Y. C. Fang, and C. R. Appledorn, Med. Phys. **22**, 1605 (1995).
[8]Y. Wang, D. Xing, Y. G. Zeng, and Q. Chen, Phys. Med. Biol. **49**, 3117 (2004).
[9]K. P. Köstli and P. C. Beard, Appl. Opt. **42**, 1899 (2003).
[10]C. G. A. Hoelen and F. F. M. Mul, Appl. Opt. **39**, 5872 (2000).
[11]C. K. Liao, M. L. Li, and P. C. Li, Opt. Lett. **29**, 2506 (2004).
[12]M. H. Xu and L.-H. V. Wang, IEEE Trans. Med. Imaging **21**, 814 (2002).
[13]X. Wang, Y. Pang, G. Ku, X. Xie, G. Stoica, and L.-H. V. Wang, Nat. Biotechnol. **21**, 803 (2003).
[14]D. W. Yang, D. Xing, H. M. Gu, Y. Tan, Y. Tan, and L. M. Zeng, Appl. Phys. Lett. **87**, 194101 (2005).
[15]Y. G. Zeng, D. Xing, Y. Wang, B. Z. Yin, and Q. Chen, Opt. Lett. **29**, 1760 (2004).